Improved discrimination of subglacial and periglacial erosion using [10]Be concentration measurements in subglacial and supraglacial sediment load of the Bossons glacier (Mont Blanc massif, France)

Hervé Guillon,[1,2]* Jean-Louis Mugnier,[1,2] Jean-François Buoncristiani,[3,4] Julien Carcaillet,[2,5] Cécile Godon,[1,2] Charlotte Prud'homme,[1,2] Peter van der Beek[2,5] and Riccardo Vassallo[1,2]
[1] Université de Savoie, ISTerre, F-73376 Le Bourget du Lac, France
[2] CNRS, ISTerre, F-73376, Le Bourget du Lac, France
[3] Université de Bourgogne, Biogéosciences, F-21000 Dijon, France
[4] CNRS, Biogéosciences, F-21000 Dijon, France
[5] Université Grenoble Alpes, ISTerre, F-38041 Grenoble, France

ESPL

Earth Surface Processes and Landforms

ABSTRACT: Deciphering the complex interplays between climate, uplift and erosion is not straightforward and estimating present-day erosion rates can provide useful insights. Glaciers are thought to be powerful erosional agents, but most published 'glacial' erosion rates combine periglacial, subglacial and proglacial erosion processes. Within a glaciated catchment, sediments found in subglacial streams originate either from glacial erosion of substratum or from the rock walls above the glacier that contribute to the supraglacial load. Terrestrial cosmogenic nuclides (TCN) are produced by interactions between cosmic ray particles and element targets at the surface of the Earth, but their concentration becomes negligible under 15 m of ice. Measuring TCN concentrations in quartz sand sampled in subglacial streams and in supraglacial channels is statistically compliant with stochastic processes (e.g. rockfalls) and may be used to discriminate subglacial and periglacial erosion. Results for two subglacial streams of the Bossons glacier (Mont Blanc massif, France) show that the proportion of sediments originating from glacially eroded bedrock is not constant: it varies from 50% to 90% ($n = 6$). The difference between the two streams is probably linked to the presence or absence of supraglacial channels and sinkholes, which are common features of alpine glaciers. Therefore, most of the published mean catchment glacial erosion rates should not be directly interpreted as subglacial erosion rates. In the case of catchments with efficient periglacial erosion and particularly rockfalls, the proportion of sediments in the subglacial stream originating from the supraglacial load could be considerable and the subglacial erosion rate overestimated. Here, we estimate warm-based subglacial and periglacial erosion rates to be of the same order of magnitude: 0.39 ± 0.33 and 0.29 ± 0.17 mm a^{-1}, respectively. Copyright © 2015 John Wiley & Sons, Ltd.

KEYWORDS: cosmogenic nuclides; erosion rate; glacial erosion

Introduction

Deciphering the complex interplays between uplift, erosion and relief (e.g. Molnar and England, 1990) requires quantifying accurately each process involved. Glacial erosion plays a major role in the formation of surface relief (Montgomery, 2002; Champagnac *et al.*, 2012) and has been argued to be an extremely efficient erosional process that can lead to erosion rates greater than 10 mm a^{-1} (Hallet *et al.*, 1996; Koppes and Montgomery, 2009). Numerical models (e.g. Pedersen and Egholm, 2013; Sternai *et al.*, 2013) recently highlighted the important role of glacial erosion in shaping the topography of mid-latitude mountain ranges, but the erosion laws

applied call for more *in situ* erosion rate data to better calibrate their parameters.

A common methodology to estimate present-day erosion rate (LT^{-1}) within a glaciated catchment is based on measuring sediment flux (MT^{-1}) in a subglacial stream and relating it to the catchment area (L^2) and to the density of the eroded rocks (ML^{-3}). Numerous authors have used this methodology; results have been compiled by Hallet *et al.* (1996), Delmas *et al.* (2009) and Hinderer *et al.* (2013). For the Alps, the latter authors reported erosion rates of glaciated catchments to range from 0.007 to 2.87 mm a^{-1} with a mean value of 0.24 mm a^{-1} ($n = 116$). These values, like most published 'glacial' ero-

sion rates, are catchment-averaged erosion rates that pertain to subglacial, periglacial and proglacial erosion processes.

Erosion within a glaciated catchment is a combination of periglacial, glacial and proglacial erosion processes (e.g. Benn and Evans, 2010; Slaymaker, 2011). Periglacial erosion processes (e.g. frost cracking, gelifluction, rockfalls induced by permafrost thaw) are dominated by frost action and can occur in a non-glaciated catchment. Subglacial processes (e.g. plucking, basal sliding abrasion, chemical weathering) take place at the base of a glacier and are directly related to glacial dynamics. Proglacial processes occur within the proglacial area of a glacier and are mainly glaciofluvial, fluvial and hillslope processes. Some of these can be seen as paraglacial processes linked to an unsteady landscape resulting from the former presence of a glacier (Church and Ryder, 1972). Therefore, estimating subglacial erosion at catchment scale requires separating this process from many other processes that operate throughout the catchment.

In Alpine glacial environments, the sediment load of subglacial streams can be derived from two sources: the substratum beneath the glacier and the rock walls surmounting the glacial surface. Quantifying and discriminating subglacial erosion and periglacial erosion requires a method to determine the origin of the sediments. Here, we test the applicability of terrestrial cosmogenic nuclides (TCN) to achieve such quantification.

TCN are continuously produced in the uppermost layer of the Earth's surface by interactions between cosmic rays and target elements of the lithosphere (mainly silicon and oxygen; e.g. Lal, 1991). Among the vast diversity of TCN applications, TCN concentrations allow estimation of exposure age of preserved surfaces (e.g. Brown *et al.*, 1991) and catchment denudation rates (e.g. Brown *et al.*, 1995; Dunai and Stuart, 2009). Measuring TCN concentrations also provides avenues to estimate the mean erosion rate of the mountain slopes that supply supraglacial sediments (e.g. Heimsath and McGlynn, 2008; Ward and Anderson, 2011), to evaluate the erosion/exposure history of eroded surfaces in the vicinity of a glacier (e.g. Goehring *et al.*, 2012; Berg *et al.*, 2012) or to characterize sediment transfer processes (e.g. Delunel *et al.*, 2014). TCN production rate exponentially decreases with depth and is negligible beneath ∼5 m of rocks or ∼15 m of ice (Appendix, Figure A1), which suggests TCN concentration measurements have the potential to differentiate sediments originating from the ice-covered substratum (with low or negligible TCN concentrations) and sediments provided by ice-free slopes (with TCN concentrations depending on periglacial slope erosion rates).

The aim of this paper was to test the use of TCN concentrations of glacial sediments in order to discriminate their sources and associated erosion processes (subglacial versus periglacial erosion). A recent study (Godon *et al.*, 2013) used sediment grain size distribution and U-Pb ages of detrital zircons to establish sediment sources and calculate relative erosion rates of the different reservoirs within the Bossons glacier catchment (Mont Blanc Massif, Western Alps). Working in the same
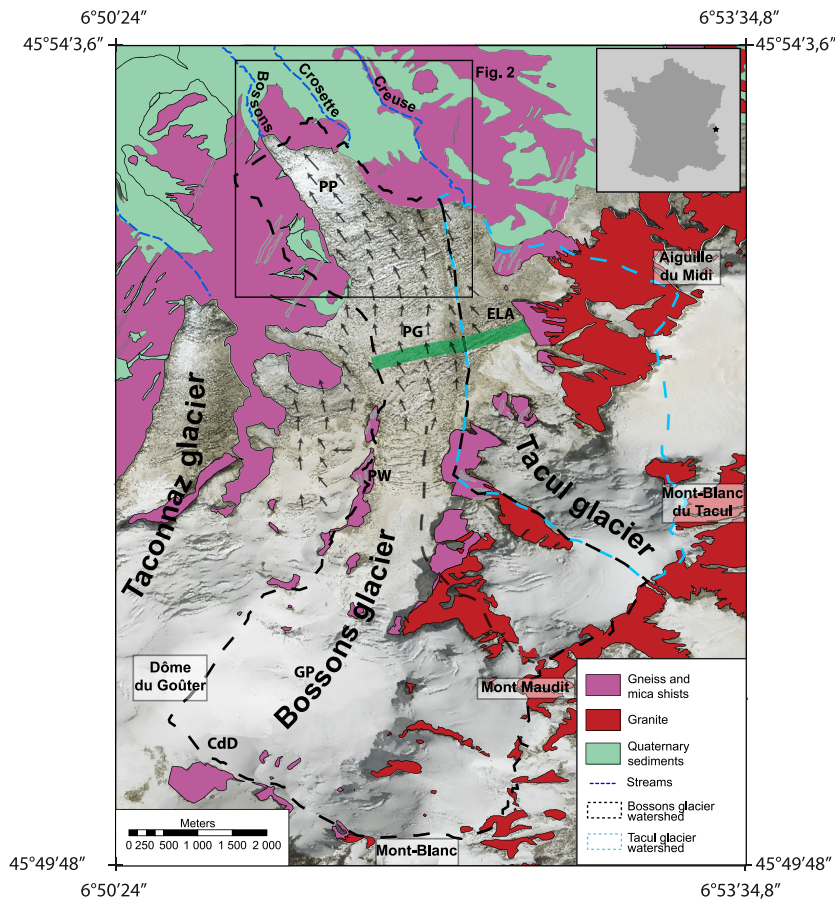
Figure 1. Map showing the glacier system and simplified bedrock geology around Mont Blanc. Inset shows location in France. The proglacial Creuse, Crosette and Bossons streams are also indicated. ELA, equilibrium line altitude (after Godon *et al.*, 2013). Subglacial catchment limits (dashed lines) have been mapped (Godon, 2013) using a hydrological model (GSM-Socont, Schaefli *et al.*, 2005) and geomorphological evidence. Black arrows represent ice flow direction estimated from TerraSAR-X data (Fallourd *et al.*, 2011). Location of Plateau des Pyramides (PP), Plan Glacier (PG), Col du Dôme (CdD), Grand Plateau (GP) and Pic Wilson (PW) are specified. Box indicates location of Figure 4. This figure is available in colour online at wileyonlinelibrary.com/journal/espl

area, we sampled sediments from several outlets of subglacial meltwater streams as well as the supraglacial sediment load, in which we analyzed *in situ*-produced cosmogenic [10]Be concentrations. The results are interpreted and compared in terms of sediment sources, erosion processes and erosion rates.

Setting and Methods

Setting

The Bossons glacier flows down the north face of Mont Blanc in the French Western Alps (Figure 1). Its source covers Mont Blanc, the highest summit of western Europe at 4810 m above sea level (asl), and the glacier extends down to an altitude of 1450 m asl. The Tacul glacier is the main glacial tributary of the Bossons glacier.

Both are polythermal glaciers and the temperature distribution of their basal ice is probably very complex. Vincent *et al.* (2007) reported −11°C at the bottom of a 140 m deep borehole reaching bedrock in the upper part of Bossons glacier (4250 m asl, Col du Dôme) and in 1998 firn was cold down to 3920 m asl on Bossons glacier (Suter, 2001). The thermal structure of the Bossons glacier is thought to be similar to that reported for other European Alpine glaciers (Haeberli, 1976; Suter and Hoelzle, 2002): a high and cold accumulation area and a lower and temperate ablation area (type D according to the classification of Blatter and Hutter, 1991). Observations at the base of seracs on the nearby Taconnaz glacier (Figure 1) suggest that the transition between cold and temperate basal ice occurs at a maximum altitude of 3300 m asl (Le Meur and Vincent, 2006).

The equilibrium line altitude (ELA) was estimated at ∼2750 m asl on the Bossons glacier (Figure 1; Godon *et al.*, 2013) and separates accumulation and ablation areas. Within the former, supraglacial clasts are buried under snow, firn and ice (relative downward movement to the glacial surface), whereas in the latter clasts are exhumed by ice and snow loss (relative upward movement). Melting and hydrofracturing can create englacial drainage that may reach the substratum and connect supraglacial and subglacial drainage systems (van der Veen, 2007; Benn *et al.*, 2009). The Bossons glacier is steep (mean slope gradient: 0.49) but has two flat sections: Plan Glacier at ∼2300 m asl and Plateau des Pyramides at ∼1800 m asl. On the latter, once snow cover has disappeared by ablation leaving impermeable ice, rainfall run-off and meltwater form sheet flow or follow supraglacial channels.

The subglacial hydrological network beneath the Bossons glacier has three outlets, which are located at altitudes of 2300 m asl (Creuse stream), 1760 m asl (Crosette stream) and 1450 m asl (Bossons stream), respectively (Figure 1). Godon *et al.* (2013) mapped subglacial catchments for each of the subglacial streams using geomorphological evidence and a hydrological model (Schaefli *et al.*, 2005). The Creuse stream mainly drains the Tacul glacier (Figure 1), the Crosette stream drains the upper part of the Bossons glacier (1.43 km^2 beneath temperate ice and 5.64 km^2 beneath cold ice) and the lowest outlet, the Bossons stream, collects meltwater from a relatively small catchment (0.38 ± 0.12 km^2) with temperate basal ice and below the ELA.

Huss and Farinotti (2012) inferred ice thickness of the Bossons glacier from glacial surface topography and ice dynamics. The glacier is thought to be between 30 and 180 m thick, with a mean ice thickness of ∼60 m (Huss and Farinotti, 2012; Huss, personal communication; Figures A2 and A3). Those finding are consistent with the 140 m deep Col du Dôme borehole Vincent *et al.* (2007) and field observations. Thickest sections of the Bossons glacier are located in over-deepened areas, while the glacier thins toward its side or near rock islets.

The bedrock of the Bossons glacier catchment is dominated by two different units: a Variscan polymetamorphic basement and the younger Mont Blanc calc-alkaline granite, which intruded the former. Both lithologies are easily told apart and the boundaries of the granitic pluton can be interpolated beneath the glacier between outcrops that are separated by less than 500 m (Figure 1). These rock islets are mainly granitic (0.335 km^2 of granites and 0.126 km^2 of polymetamorphic rocks) but, beneath the ELA, the slopes surmounting the glacier are formed exclusively by polymetamorphic rocks. Large moraines linked to the Little Ice Age (LIA) extent of the Bossons glacier (Nussbaumer and Zumbühl, 2012) are present in the proglacial area at least at 500 m from the glacial tongue and cannot supply sediment to the glacier. Extensive fieldwork by (Godon *et al.*, 2013) showed no evidence of upward englacial transport (e.g. no englacial thrusting). Most of the supraglacial load is therefore provided by rockfalls occurring on the steep slopes surmounting the glacier.

The origin of coarse clasts is easily established by petrographic inspection. For smaller grain sizes, the age difference between the ∼303 Ma (Bussy *et al.*, 1989) Mont Blanc granite and the older (∼450 Ma and 320–327 Ma; Paquette *et al.*, 1989; Bussy *et al.*, 2000) polymetamorphic basement can be employed. Godon *et al.* (2013) applied detrital-zircon U-Pb geochronology to decipher the origin of sediments in two subglacial streams of the Bossons glacier (Bossons and Crosette).

Rockfalls stochastically renew the exposed rock wall surfaces, leading to variable ages for the rock walls (Parker and Perg, 2005). As a result, exposure ages between 1.47 ± 0.14 and 38.6 ± 1.20 ka have been found for the ∼3800 m asl Aiguille du Midi crests ∼6 km NE of the Bossons glacier (Böhlert *et al.*, 2008; Figure 1 and Table I). Younger exposure ages (less than 1.51 ± 0.26 ka; Prud'homme, 2013; Table I) were reported for a several-meter-sized granite block located on the Bossons glacier. Such a difference in exposure ages can be linked to the nature of the sampled surface (i.e. a less exposed area or a more intensely rejuvenated one) or to glacial transport during which mechanical erosion prevents the most exposed face being preserved.

Within the glacier, clast transport takes place at the rate of the glacier motion; space radar (TerraSAR-X) observations indicate velocities locally as high as 1.4 m d^{-1} (Fallourd *et al.*, 2011). On a longer timescale, debris from aircraft that crashed near the summit of Mont Blanc in 1950 and 1966 and corpses of unfortunate alpinists were transported to the front of the 12 km long Bossons glacier in less than 50 years (Vivian, 1969; Rey, 2004).

Sampling strategy

Supraglacial TCN concentration variability seems non-negligible from the few non-morainic supraglacial data published. Seong *et al.* (2009) reported supraglacial [10]Be concentrations ranging from 4.22 ± 0.36 to 15.5 ± 0.75 × 10^4 atoms g^{-1} for samples from the ∼58 km long Baltoro Glacier (K2 area, Karakoram, Pakistan). For the much smaller (∼3 km long) Milarepa Glacier (Annapurna, Nepal), Heimsath and McGlynn (2008) reported concentrations ranging from 0.24 ± 0.15 to 5.72 ± 0.9 × 10^4 atoms g^{-1}. In each study, mean sample concentration is approximately twice the sample standard deviation: 6.77 ± 3.32 × 10^4 atoms g^{-1} and 2.24 ± 1.70 × 10^4 atoms g^{-1}, respectively ($\bar{X}$ ± s). Such deviations require the use of several samples when studying periglacial or subglacial processes through TCN measure-

Table I. TCN results for Bossons glacier and nearby Aiguille du Midi

Sample	Location	Latitude (°N)	Longitude (°E)	Altitude (m asl)	$^{10}Be/^9Be^a$	^{10}Be concentration (atoms g^{-1})	Uncertainty[b] (atoms g^{-1})
AdM1*	Aiguille du Midi rock walls	~ 45°53′17.60″	~ 6°52′42.10″	3800	NC	1.58×10^6	4.73×10^4
AdM2*	Aiguille du Midi rock walls	~ 45°53′17.60″	~ 6°52′42.10″	3810	NC	6.03×10^4	5.55×10^3
AdM3*	Aiguille du Midi rock walls	~ 45°53′17.60″	~ 6°52′42.10″	3750	NC	2.42×10^5	1.21×10^4
AdM4*	Aiguille du Midi rock walls	~ 45°53′17.60″	~ 6°52′42.10″	3740	NC	2.48×10^5	1.14×10^4
AdM5*	Aiguille du Midi rock walls	~ 45°53′17.60″	~ 6°52′42.10″	3740	NC	2.83×10^5	1.47×10^4
CRO2**	Crosette roches moutonnées	45°53′29.06″	6°51′33.05″	1762	1.45×10^{-14}	1.31×10^4	5.98×10^3
CRO4**	Crosette roches moutonnées	45°53′29.07″	6°51′33.08″	1763	1.16×10^{-14}	8.30×10^3	4.23×10^3
BOS2A	Bossons subglacial stream	45°53′31.92″	6°51′8.78″	1443	1.23×10^{-14}	1.52×10^4	2.40×10^3
BOS2B	Bossons subglacial stream	45°53′31.92″	6°51′10.04″	1441	1.16×10^{-14}	1.10×10^4	2.82×10^3
BOS8	Bossons stream datalogger	45°53′57.84″	6°50′56.11″	1240	1.60×10^{-14}	1.65×10^4	2.69×10^3
BOS11	Crosette sand	45°53′30.84″	6°51′36.11″	1735	2.40×10^{-15}	2.12×10^3	6.11×10^2
Boss sous	Crosette subglacial stream	45°53′29.04″	6°51′33.01″	1760	3.31×10^{-15}	2.53×10^3	8.77×10^2
Boss supra	Supraglacial load	45°53′17.88″	6°51′16.74″	1795	2.08×10^{-14}	2.72×10^4	2.40×10^3

Results from *Böhlert *et al.* (2008) and **Prud'homme (2013) are provided for completeness. The following remarks only apply to the results of this study:

[a]AMS analysis has been performed at the French AMS facility ASTER. ^{10}Be concentrations were calibrated using the NIST Standard Reference Material 4325. Its assigned $^{10}Be/^9Be$ is 2.79×10^{-11}. No topographic shielding or cover correction has been applied. Concentrations have been corrected from the chemical blank ($^{10}Be/^9Be_{blank} = 3.31 \pm 0.76 \times 10^{-15}$).

[b]Propagated uncertainties include counting statistics, a conservative estimate of 1% for instrumental variability, the uncertainty of the standard deviation and chemical blank.

ments to take into account their stochasticity and spatial variability. For example, Ward and Anderson (2011) took samples at a regular pace along the medial moraine of a glacier and mixed them, giving venues to take into account stochastic erosion processes that are providing material to moraines.

Conversely, studies focusing on fluvial processes follow the 'let the nature do the averaging' principle and typically use only one sand sample per catchment to infer erosion rates (e.g. Brown *et al.*, 1995; von Blanckenburg, 2005; Delunel *et al.*, 2010; Derrieux *et al.*, 2014; Scherler *et al.*, 2014). Concerns about grain size-dependent (e.g. Brown *et al.*, 1995; Carretier *et al.*, 2013; Aguilar *et al.*, 2014; see Codilean *et al.*, 2014, for data review) or process-dependent (e.g. Delunel *et al.*, 2014) TCN concentrations are not relevant when the goal is to decipher sediment sources from samples of identical grain size. Poor sediment mixing (e.g. Savi *et al.*, 2014) can significantly impact TCN concentrations and their implications. However, mixing processes may be analogous both in fluvial drainage systems and in supraglacial channels fed by rainfall run-off and meltwater and sampling as far downstream as possible favors efficient mixing (Savi *et al.*, 2014).

During englacial transfer, the viscous flow of the glacier impedes clast crushing and lateral sediment mixing. Nonetheless, below the ELA, ablation concentrates clasts at the surface, leading to vertical mixing of different sources in the supraglacial load (Figure 2). On Bossons glacier, frost cracking of the coarser supraglacial clasts produces additional fine particles, which are transported and mixed by supraglacial sheet flow or within incised channels. Such fluvial processes dominating supraglacial debris distribution may not be valid in a wide range of existing supraglacial environments in which more diffusive mechanism (e.g. table-topple mechanism; Anderson, 2000) may dominate. Nonetheless, in the case of Bossons glacier, sampling fine particles in a supraglacial channel draining an area as large as possible, and as far down on the glacier as possible to maximize mixing, appears statistically acceptable.

In this paper, we use the same sand samples that were previously analyzed by Godon *et al.* (2013) for detrital zircon (U-Pb) geochronology in order to compare the two methods. Samples have been collected in subglacial cavities (Figure 3c) at the outlets of the Bossons (BOS2A, BOS2B) and Crosette

(Boss sous) streams. Sand particles were also collected downstream along these two streams (Figure 3a; BOS8 and BOS11 at 1130 and 80 m from the glacial front, respectively) and from supraglacial sediments (Figure 3b, Boss supra). Moreover, two roches moutonnées were sampled in order to test TCN inheritance of the substratum (Figure 3a, CRO2 and CRO4). Sample details are provided in Table I, while Figures 3 and 4 show field setting and sample locations.

Medium-sand particles were separated by sieving; samples were not crushed. Godon *et al.* (2013) determined that such fine particles represent only 5% of the total supraglacial load, which is highly heterogeneous but dominated by very coarse particles. Roches moutonnées samples, which were collected from a superficial rock layer of a few centimeters thick, were crushed and sieved to retrieve the 80–500 µm grain size. Zircons were retrieved from the 80–200 µm fraction for detrital (U-Pb) geochronology (Godon *et al.*, 2013), whereas TCN concentrations were measured on quartz from the 200–500 µm fraction. After this initial crushing and separation stage, 200 g of each sample were selected for further preparation.

^{10}Be concentration measurements

Beryllium oxide targets were extracted from sand samples following the chemical procedures of Brown *et al.* (1991) and Merchel and Herpers (1999). Extractions were performed at the Institut des Sciences de la Terre (Grenoble, France) from ~20 g of quartz for each sample. ^{10}Be concentrations were measured at the French national accelerator–mass spectrometry (AMS) facility ASTER (Aix-en-Provence, France) (Arnold *et al.*, 2010). They were calibrated against NIST Standard Reference Material 4325 using its assigned $^{10}Be/^9Be$ ratio of 2.79 ± 0.0310^{-11} and a ^{10}Be half-life of 1.387 ± 0.012 Ma (Chmeleff *et al.*, 2010; Korschinek *et al.*, 2010). Ages were calculated using the online Cronus calculator (Balco *et al.*, 2008) and concentrations have been corrected for the chemical blank ($^{10}Be/^9Be$ blank = $3.31 \pm 0.76 \times 10^{-15}$). Topographic shielding and cover corrections are usually applied in order to estimate exposure times; however, as we mainly use the ^{10}Be concentration as a provenance indicator, we refrain from such corrections. As concentrations are relevant to characterize the sources, exposure age estimations have only been
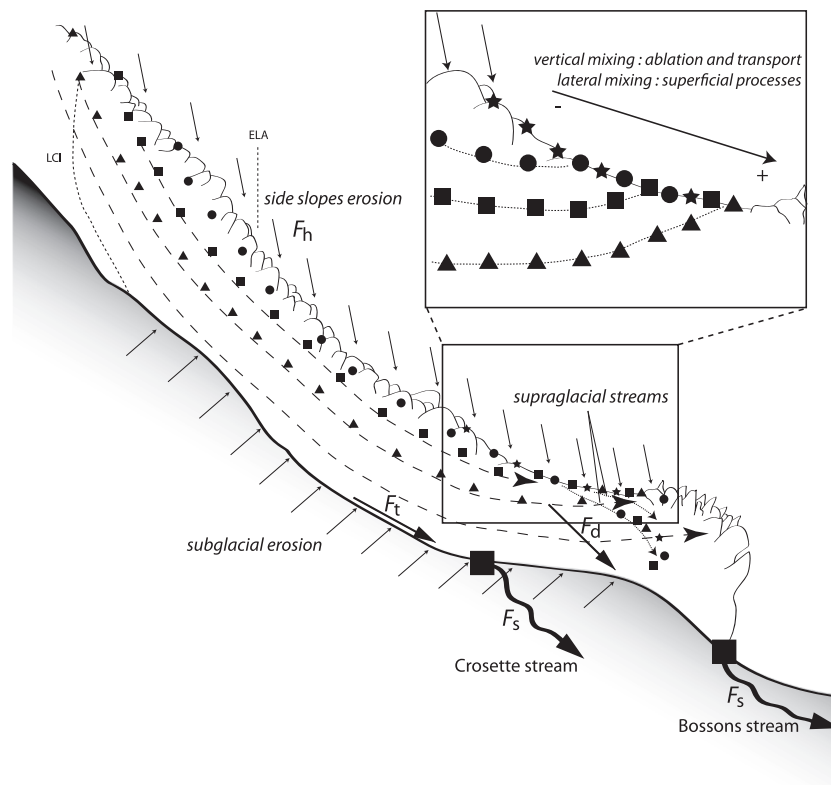
Figure 2. Sketch of the clast flux in a glacial environment. Clasts supplied by hillslope erosion (F_h) are either incorporated into the glacier (F_d) or delivered to the lateral moraines. Above the ELA, clasts follows flow lines and finally reach the surface of the glacier due to ablation below the ELA. Inset: symbols refer to the source of the clasts. Vertically mixed supraglacial clasts move at the same velocity as the glacier; however, clast movement and mixing in lateral inputs are favored by superficial processes (i.e. sliding favored by ablation, supraglacial sheet flow, transport in incised channels). Moulins and cracks connect supraglacial channels and subglacial drainage, providing part of the supraglacial sediment load to the subglacial stream. Sediment load in subglacial stream (F_s) is thus a mixture of two components: erosion at the base of the temperate glacier (F_t) and sediments supplied by hillslope erosion and incorporated into the glacier (F_d).

carried out for the roche moutonnée samples. Thickness scaling and topographic shielding have been applied but no snow cover correction was performed.

Results and discussion

Results

Maximum TCN concentrations (Table I) are found in the supraglacial load (2.72×10^4 atoms g^{-1}). By comparison, ^{10}Be concentration of sand collected from the Crosette stream is an order of magnitude lower (2.53×10^3 atoms g^{-1}) and their uncorrected ^{10}Be/^{10}Be ratio (6.62×10^{-15}) is close to the blank level (3.31×10^{-15}). Conversely, ^{10}Be concentrations of sediments collected from the Bossons subglacial stream (1.10 and 1.50×10^4 atoms g^{-1}) are significantly above the measurement blank.

The sediment load of the proglacial stream has been sampled ~1 km downstream from the glacier front and its ^{10}Be concentration is not significantly different (1.60×10^4 atoms g^{-1}) from those measured in the Bossons subglacial stream sediments. Such similarity may be linked to run-off washing out from the lateral moraines and providing material to the proglacial stream. The lack of ^{10}Be enrichment (2.12×10^3 atoms g^{-1}) for the sample collected in the Crosette stream ~80 m downstream of the glacier indicates that very little sand is added to the stream from supraglacial load at the front of the glacier.

Exposure of the glacier substratum during periods of glacial retreat

Direct determination of the ^{10}Be concentration of the substratum beneath the glacier is not possible but the spallation reactions that mainly control the concentration of ^{10}Be in crustal rocks are strongly attenuated beneath earth surface materials (e.g. rock, ice). A secondary ^{10}Be production mechanism is by fast and negative muon interactions (Bilokon et al., 1989; Heisinger et al., 1997; Dunai, 2010). These particles have a much greater penetration depth, so nuclides may be significantly produced even under ice cover. However, because the fraction of muons in the cosmic ray spectrum is very small (~2% at the Earth's surface; Braucher et al., 2003), production of ^{10}Be by muons does not significantly affect the TCN concentrations (see Goehring et al., 2012; Figure A1).

We can estimate the mean ^{10}Be production rate below the Bossons glacier using Huss and Farinotti (2012) thickness data and TCN production relations (Lal, 1991; Stone, 2000; Heisinger et al., 2002a, 2002b; Braucher et al., 2003; Balco et al., 2008; Appendix). For 98% of the surface beneath the glacier, the production is less than 1 atom g^{-1} a^{-1} (Figure 5). The mean production rate beneath the present-day glacier averaged over the Holocene (~12 ka) yields a concentration of 3.96×10^3 atoms g^{-1}. It is clear that the ^{10}Be concentration measured in the Crosette subglacial stream sediments (2.53×10^3 atoms g^{-1}) is close to this mean calculated concentration and excludes significant input of ^{10}Be enriched sediment. Nonetheless, this calculation neglects the fluctuations of glacier extent or thickness.
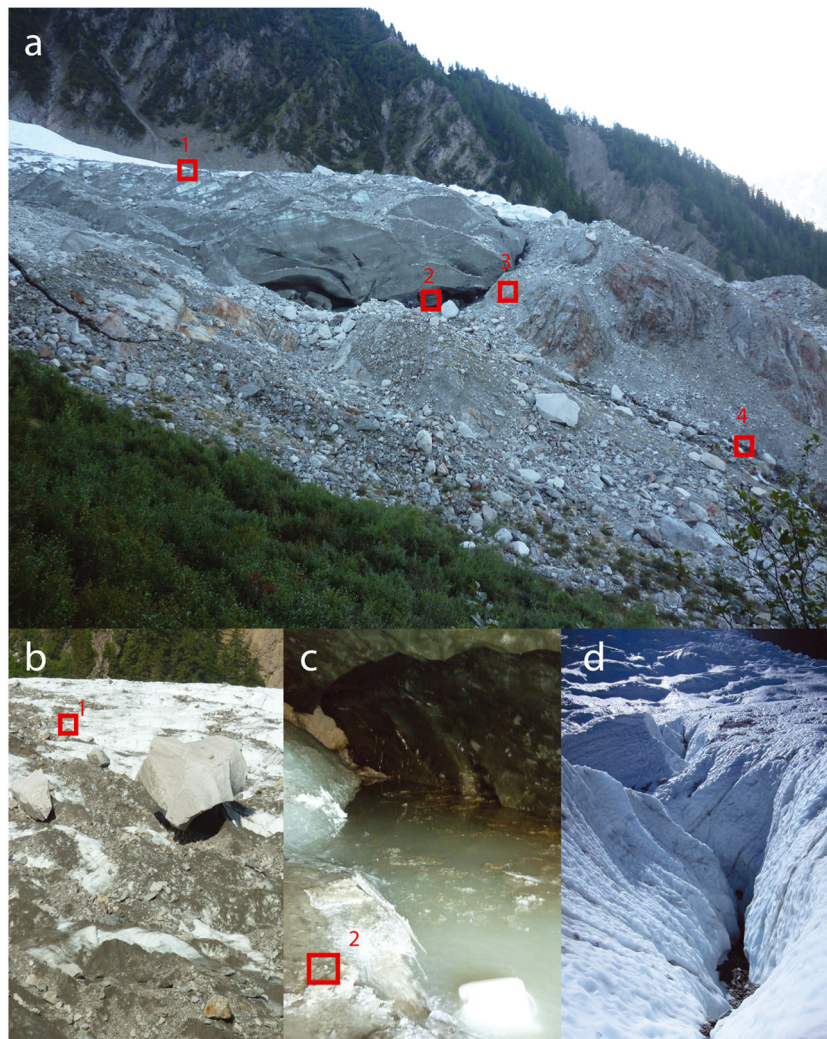
Figure 3. Field photos of sample locations. (a) Bossons glacier close to Crosette stream; boxes show sample sites: (1) supraglacial load carried by the Bossons glacier (sample 'Boss supra'); (2) Crosette subglacial stream sediments (sample 'Boss sous', collected in the ice cave beneath the glacier); (3) roche moutonnée (samples 'CRO2 and CRO4'); (4) sediment of the Crosette stream (sample 'BOS11') downstream of the outlet. Block near (2) is ∼5 m wide. (b) Close-up view of the supraglacial load of the Bossons glacier (sampling site 1 indicated). Biggest block is ∼5 m wide. (c) Close-up view of the outlet of the Crosette subglacial stream (sampling site 2 indicated). Cavity is ∼5 m deep. (d) Supraglacial stream above the Bossons glacier (cf. inset in Figure 4). Water flows ∼5 m below glacial surface. This figure is available in colour online at wileyonlinelibrary.com/journal/espl

The Bossons glacier has been retreating rapidly since the LIA (Nussbaumer and Zumbühl, 2012) due to its steepness and high elevation difference between head and terminus, and it should react very dynamically to future climate changes (Roe and O'Neal, 2005; Lüthi and Bauder, 2010). Therefore, repeated exposure of the substratum below the lower part of the glacier during the Holocene climatic optima that postdate the Last Glacial Maximum cannot be excluded. Two measurements on roches moutonnées near the glacier front at 1760 m asl yield TCN concentrations of 1.31×10^4 and 8.30×10^3 atoms g^{-1}, respectively (Figure 4 and Table I). Assuming there is no erosion, apparent exposure ages are found to be between 1.21 ± 0.55 ka and 0.47 ± 0.24 ka, suggesting that the glacier has recently retreated during a relatively long period beyond its current snout location (1.5 km from LIA maximum extent). Goehring *et al.* (2011) measured exposure ages between 1.2 and 5.3 ka for polished bedrock at ∼2250 m asl in front of the Rhone glacier (Switzerland) and suggested that the Rhone glacier was smaller than today for most of the Holocene. Conversely, Dielforder and Hetzel (2014) reported an apparent exposure age of 0.26 ± 0.04 ka for a recently exposed bedrock surface located at the snout of the Chaltwasser glacier (Simplon pass, Switzerland) at 2776 m asl and made the assumption that cosmogenic inheritance in their samples is negligible.

The difference between TCN concentrations measured in the subglacial stream and in a recently exposed bedrock surface located at the snout of the glacier can be linked to negligible current erosion of proglacial deglaciated substratum preserving ^{10}Be inheritance in roches moutonnées. Such difference may be qualitatively related to two glacial retreat scenarios: (i) a short paleo-exposure time preventing significant ^{10}Be enrichment (Figure 6a) or (ii) a longer paleo-exposure time but a limited glacial paleo-retreat so that the area of the ^{10}Be-enriched proglacial bedrock (l) is negligible with respect to the subglacial drainage area (L, Figure 6b).

Origin of subglacial stream sediments

Sediments supplied by hillslope erosion (F_h, hillslopes) are either incorporated into the glacier (F_d, downward) or delivered to the lateral moraines (F_m, moraines, Figure 2). Sediment load in subglacial stream (F_s, stream) is a mixture of two components: erosion at the base of the temperate glacier (F_t, temperate) and sediments supplied by hillslope erosion and incorporated into the glacier (F_d). Transport from the base
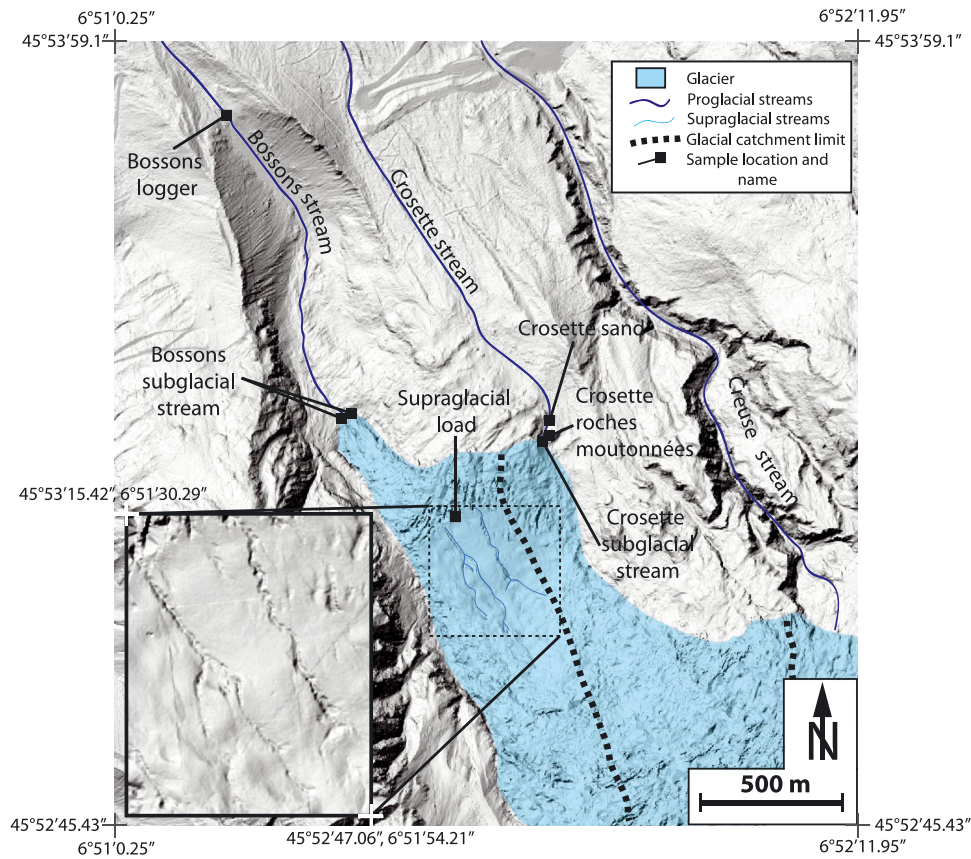
Figure 4. Shaded relief map of the lower part of the Bossons glacier, based on 1 m resolution airborne Lidar data collected in 2008 (IRSTEA, unpublished). Thick dashed lines show subglacial watershed limits as in Figure 1. Supraglacial channels and sinkholes are only present above the subglacial watershed of the Bossons stream. Sampling locations for TCN samples are indicated by black squares. Detailed information including TCN concentration for each sample can be found in Table I. This figure is available in colour online at wileyonlinelibrary.com/journal/espl

towards the top of the glacier and glacial erosion under cold ice were found to be negligible in the Bossons glacier (Godon *et al.*, 2013). Assuming steady state and no subglacial sediment storage, the mixing Equation (1) governs the sediment flux (F_s) at the outlet of the Bossons subglacial streams:

$$F_s = F_t + F_d \tag{1}$$

In addition, the granite proportion G_s and ^{10}Be concentration in the subglacial stream sediments should stem from the mixing of two poles: substratum and supraglacial load. The proportion C of sediment derived from the supraglacial load in the sediment load of the stream ($C = F_d/F_s$) can be inferred using the following similar equations:

$$\left[^{10}Be\right]_s = C \times \left[^{10}Be\right]_d + (1 - C) \times \left[^{10}Be\right]_t \tag{2}$$

$$G_s = C \times G_d + (1 - C) \times G_t \tag{3}$$

where $\left[^{10}Be\right]$ and G represent ^{10}Be concentration and granite proportion, respectively, and the subscripts s, d and t indicate the subglacial stream load, the supraglacial load and the substratum, respectively.

The substratum ^{10}Be concentration is found to be negligible ($\left[^{10}Be\right]_t = 0$; see Appendix) and both subglacial Bossons and Crosette catchments under temperate ice are entirely in metamorphic basement rocks ($G_t = 0$). Hence relations (2) and (3) become

$$\left[^{10}Be\right]_s = C \times \left[^{10}Be\right]_d \tag{4}$$

$$G_s = C \times G_d \tag{5}$$

C can then be calculated using the concentrations reported in Tables I and II. In the Bossons subglacial stream, we estimate 48±14% of the sediments to derive from the supraglacial load, whereas in the Crosette subglacial stream only 9 ± 4.5% of the sediments are derived from supraglacial load (Table II). Evaluation of the variability of ^{10}Be concentration
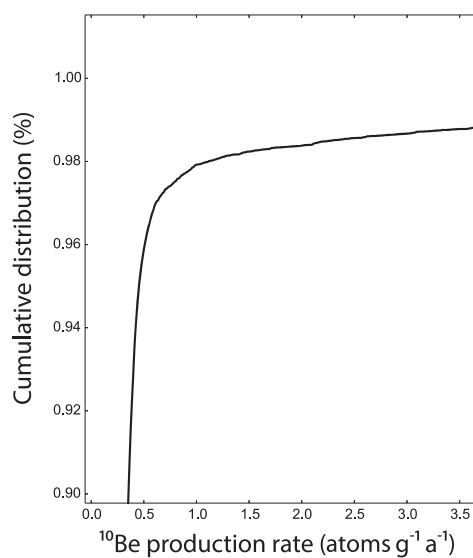
Figure 5. Cumulative distribution of ^{10}Be production rate under Bossons glacier inferred from the Huss and Farinotti (2012) ice thickness model. Less than 2% of the ice-covered substratum has a production rate higher than 1 atom g^{-1} a^{-1}. Details are given in the Appendix.
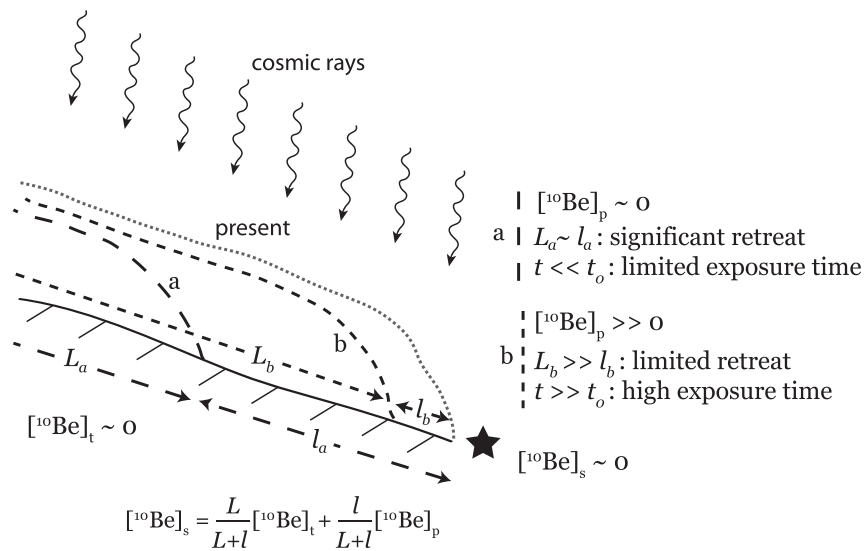
Figure 6. Negligible ^{10}Be concentration in stream load related to glacial retreat scenarios. Ice-covered bedrock ^{10}Be concentration ($[^{10}\text{Be}]_t$) is negligible whereas the concentration in proglacial bedrock $\left([^{10}\text{Be}]_p\right)$ may not be. The black star represents a measurement location within a stream. L is the stream length beneath the glacier whereas l is the one within the proglacial area. (a) Short exposure time preventing significant ^{10}Be enrichment. (b) Limited glacial retreat so that ^{10}Be-enriched proglacial area is negligible with respect to subglacial catchment area.

in supraglacial sand is the topic of ongoing research but only one supraglacial was used in this analysis (following the 'let the nature do the averaging principle'). Our results may thus be impacted by higher uncertainties than what the analytical uncertainties suggest.

Nonetheless, Godon *et al.* (2013) measured G_s using U-Pb dating on 75 zircons. Using their zircon-age data and their methodology to calculate granite proportion in each samples (Appendix E from Godon *et al.*, 2013) shows that less than 10% of the fine-grained sediments in the Crosette stream are derived from the supraglacial load, whereas this proportion reaches $\sim$ 35% for the Bossons stream sediments (Table II).

Therefore, both independent estimates of sediment provenance for these two streams are coherent. The significant correlation between normalized granite proportions and normalized ^{9}Be concentrations (Figure 7) supports the applicability of the mixing hypothesis (2).

The difference between the two streams is thought to be linked to the distinct position of their catchments. A large part of the glacier located above the Bossons subglacial catchment is characterized by supraglacial streams and sinkholes (Figure 3d) that feed the Bossons subglacial stream in sediments coming from the supraglacial load. In contrast, the Crosette subglacial stream only flows under the hummocky and crevassed part of the glacier (Figure 4), with diffuse connectivity between the glacier surface and bedrock.

Erosion in the Bossons glacier catchment

Godon *et al.* (2013) have previously estimated erosion rates in the Bossons catchment; in the following, we refine these calculations in order to take into account our new results and estimate uncertainties and fluctuations of the erosion rate of the rock walls surmounting the glacier. Present-day (2010–2012) erosion rates of the Bossons subglacial catchment have been estimated from hydro-sedimentary monitoring of the Bossons stream (Guillon *et al.*, 2013). These indicate an annual sediment flux from the glacier (F_s) that varies between 718 ± 307 and 892 ± 246 t a^{-1}. Using the proportion C of sediment derived from the supraglacial load (Table II), the mean value of 791 ± 212 t a^{-1} can be split between subglacial and

supraglacial contributions ($F_d = C \times F_s$ and $F_t = (1 - C) \times F_s$). The erosion rate e_t beneath the temperate glacier drained by the Bossons stream is then

$$e_t = \frac{(1 - C) \times F_s}{\rho S_t} \tag{6}$$

where ρ is rock density and S_t is the subglacial catchment area. Taking $C = 0.48\pm0.14$, $F_s = 791\pm212$ t a^{-1}, $S_t = 0.38\pm0.12$ km^2 and $\rho = 2800$ kg m^{-3} yields a subglacial erosion rate e_t of 0.39 ± 0.33 mm a^{-1}.

The flux (F_h) derived from glaciated rock outcrops located above the glacier is split between the englacial downward flux F_d, and the flux towards lateral moraines F_m:

$$F_h = F_d + F_m$$

Since we cannot currently quantify F_m, we simply take

$$F_h > F_d \tag{7}$$

In addition, both F_d and F_h can be seen as the sum of each lithological source: granite (γ in the following) and metamorphic rocks (μ in the following). Taking G_d as the proportion of granite in the supraglacial load, this leads to

$$F_{h(\gamma)} + F_{h(\mu)} > F_{d(\gamma)} + F_{d(\mu)} = G_d \times F_d + (1 - G_d) \times F_d$$

where $F_{h(\gamma)}$ and $F_{d(\gamma)}$ ($F_{h(\mu)}$ and $F_{d(\mu)}$) are hillslope and downward flux of granite and metamorphic rocks, respectively.

Erosion rates can be calculated using the following relationships:

$$e_{h(\gamma+\mu)} = \frac{F_{h(\gamma+\mu)}}{S_{h(\gamma)} + S_{h(\mu)}} > \frac{F_d}{S_{h(\gamma)} + S_{h(\mu)}}$$

$$e_{h(\gamma+\mu)} > \frac{C \times F_s}{S_{h(\gamma)} + S_{h(\mu)}} \tag{8}$$

$$e_{h(\gamma)} = \frac{F_{h(\gamma)}}{S_{h(\gamma)}} > \frac{F_{d(\gamma)}}{S_{h(\gamma)}} = \frac{G_d \times C \times F_s}{S_{h(\gamma)}} \tag{9}$$

Table II. Characteristics of the supraglacial load, subglacial streams and substratum in terms of granite proportion, ^{10}Be concentration and proportion of sediment coming from the supraglacial load

Location	Granite proportion[a] (%)	Mean ^{10}Be concentration[b] (10^3 atoms g^{-1})	Proportion of sediment coming from supraglacial load	
			$C = G_s/G_d$ (%)	$C = [^{10}Be]_s / [^{10}Be]_d$ (%)
Supraglacial load (d)	72	27.2 ± 2.40	100	100
Bossons stream (s)	24.7 ± 1.9	13.1 ± 2.61	34 ± 2.6	48 ± 14
Crosette stream (s)	5.4 ± 1.4	2.33 ± 0.74	7.9 ± 1.9	8.5 ± 3.5
Substratum (t)	0	~ 0	0	0

[a]Granite proportion has been estimated by Godon *et al.* (2013) using U-Pb dating on 75 zircons and lithological identification.
[b]Mean ^{10}Be concentrations have been calculated using Boss supra sample for supraglacial load, BOS2 and BOS2B samples for Bossons stream and Boss sous and BOS11 samples for Crosette stream (Table I).
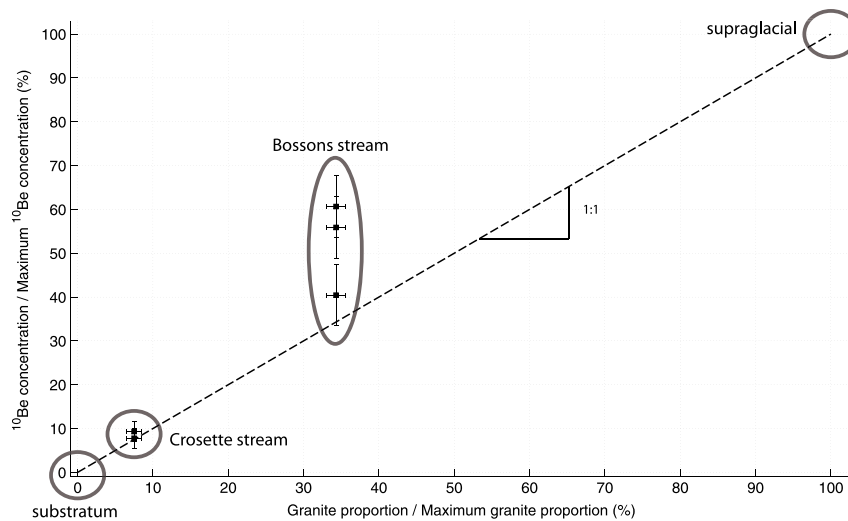
Figure 7. Comparison between granite proportion (from Godon *et al.*, 2013) and normalized ^{10}Be concentration for glacial substratum, subglacial stream sediments and supraglacial load.

$$e_{h(\mu)} = \frac{F_{h(\mu)}}{S_{h(\mu)}} > \frac{F_{d(\mu)}}{S_{h(\mu)}} = \frac{(1 - G_d) \times C \times F_s}{S_{h(\mu)}} \qquad (10)$$

where $S_{h(\gamma)}$ and $S_{h(\mu)}$ are areas of granite and metamorphic rocks outcrops, respectively.

In order to map the rock outcrops that contribute to the sediment load of the Bossons stream, we use glacier flow-lines deduced from correlation of radar images (Fallourd *et al.*, 2011) below the ELA and glacier surface slopes above the ELA. Resulting areas of granite and metamorphic rock outcrops are $S_h(\gamma) = 0.335$ km^2 and $S_h(\mu) = 0.126$ km^2, respectively. The proportion of granite G_d in the supraglacial load has been estimated by Godon *et al.* (2013) at 72%. Applying Equations (8)–(10) leads to the following erosion rates: $e_h(\gamma + \mu) > 0.29 \pm 0.17$ mm a^{-1}, $e_h(\gamma) > 0.29 \pm 0.16$ mm a^{-1} and $e_h(\mu) > 0.30 \pm 0.17$ mm a^{-1}, suggesting similar erosion for granite and metamorphic rocks.

If the supraglacial contribution to moraines were found to be negligible, subglacial ($e_t = 0.39 \pm 0.33$ mm a^{-1}) and periglacial erosion ($e_h(\gamma + \mu) > 0.29 \pm 0.17$ mm a^{-1}) would be of the same order of magnitude but the large associated uncertainties could jeopardize this apparent equality. This result would be coherent with coupled valley floor and wall lowering at similar rates (e.g. Ward and Anderson, 2011). Nevertheless, steady-state coupling between slope processes and incision at the base of the slope may be prevented by different response times of subglacial and periglacial processes to present-day glacial retreat.

Conclusions

Quantifying the relative efficiency of different erosion processes within a glaciated catchment requires differentiating the sediment flux derived from the glacier substratum from that provided by the rock walls surmounting the glacier and contributing to the supraglacial load. Because of the nearly complete reduction of cosmogenic production below a few tens of meters of ice, measurements of cosmogenic ^{10}Be concentrations appear to be a promising tool to separate sediments derived from the ice-covered bedrock from those provided by the unprotected supraglacial slopes. We have performed such ^{10}Be concentration measurements on two sub-catchments of the Bossons glacier in the Mont Blanc massif (France).

For the Crosette subglacial stream, we find a negligible ^{10}Be concentration of sand-sized stream sediments, whereas the ^{10}Be concentration on nearby roches moutonnées and supraglacial blocks are respectively 1.1×10^4 and 2.7×10^4 atoms g^{-1}. Therefore, almost 100% of the Crosette stream sediments are derived from glacial erosion of the substratum. Moreover, the erosion of the subglacial area affected by inherited exposure is negligible.

The ^{10}Be concentration in the Bossons subglacial stream sediments is $\sim 1.3 \times 10^4$ atoms g^{-1}, an order of magnitude higher than for the Crosette sediments. The difference between Bossons and Crosette subglacial stream results is interpreted as resulting from the presence of supraglacial channels and sinkholes that transfer sediments from the glacier surface to

the subglacial drainage network in the lowermost part of the Bossons glacier. Assuming that [10]Be inheritance is also negligible within the Bossons stream sub-catchment, only 50% of its sediment load would be provided by subglacial erosion. A previous estimate using U-Pb geochronology on detrital zircons sampled at the same location produced similar results (Godon *et al.*, 2013) but requires a specific lithological setting to infer sediment origin.

Supraglacial channels and sinkholes are common features of alpine glaciers. Therefore, most of the published mean catchment erosion rates for alpine glaciers should not be interpreted directly as subglacial erosion rates. In the case of catchments affected by efficient periglacial erosion, in particular rockfalls, the supraglacial component could be substantial and the subglacial erosion rate may be overestimated.

To our knowledge, this study is the first to use [10]Be concentration measurements for deciphering sediment origins in order to infer periglacial and subglacial erosion rates. For the Bossons glacier, comparable values have been found for both process erosion rates: 0.29 ± 0.17 and 0.39 ± 0.33 mm a^{-1}, respectively. Although erosion rates estimated in this study are in the range of published 'glacial' erosion rates, they cannot be compared with them. Work is still needed to take into account the periglacial, subglacial and proglacial components of erosion within studies of the sediment yield provided by glaciated catchments and TCN methods appear to be a very promising tool to achieve such discrimination.

References

Aguilar G, Carretier S, Regard V, Vassallo R, Riquelme R, Martinod J. 2014. Grain size-dependent [10]Be concentrations in alluvial stream sediment of the Huasco Valley, a semi-arid Andes region. *Quaternary Geochronology* **19**: 163–172.

Anderson RS. 2000. A model of ablation-dominated medial moraines and the generation of debris-mantled glacier snouts. *Journal of Glaciology* **46**(154): 459–469.

Arnold M, Merchel S, Bourlès DL, Braucher R, Benedetti L, Finkel RC, Aumaître G, Gottdang A, Klein M. 2010. The French accelerator mass spectrometry facility ASTER: improved performance and developments. *Nuclear Instruments and Methods in Physics Research Section B* **268**(11–12): 1954–1959.

Balco G, Stone JO, Lifton NA, Dunai TJ. 2008. A complete and easily accessible means of calculating surface exposure ages or erosion rates from [10]Be and [26]Al measurements. *Quaternary Geochronology* **3**(3): 174–195.

Benn D, Evans DJA. 2010. *Glaciers and Glaciation*. Hodder Education: Abingdon, UK.

Benn D, Gulley J, Luckman A, Adamek A, Glowacki PS. 2009. Englacial drainage systems formed by hydrologically driven crevasse propagation. *Journal of Glaciology* **55**(191): 513–523.

Berg F, Schlunegger F, Akar N, Kubik P. 2012. [10]Be-derived assessment of accelerated erosion in a glacially conditioned inner gorge, Entlebuch, Central Alps of Switzerland. *Earth Surface Processes and Landforms* **37**(11): 1176–1188.

Bilokon H, Castagnoli GC, Castellina A, Piazzoli BD, Mannocchi G, Meroni E, Picchi P, Vernetto S. 1989. Flux of the vertical negative muons stopping at depths 0.35–1000 hg/cm^2. *Journal of Geophysical Research: Solid Earth* **94**(B9): 12145–12152.

Blatter H, Hutter K. 1991. Polythermal conditions in Arctic glaciers. *Journal of Glaciology* **37**(126): 261–269.

Böhlert R, Gruber S, Egli M, Maisch M, Brandová D, Haeberli W. 2008. Comparison of exposure ages and spectral properties of rock surfaces in steep, high alpine rock walls of Aiguille du Midi, France. In *Ninth International Conference on Permafrost*, Vol. 1, Institute of Northern Engineering: University of Alaska Fairbanks, AK; 143–148.

Braucher R, Brown E, Bourlès D, Colin F. 2003. In situ produced [10]Be measurements at great depths: implications for production rates by fast muons. *Earth and Planetary Science Letters* **211**(3–4): 251–258.

Brown ET, Edmond JM, Raisbeck GM, Yiou F, Kurz MD, Brook EJ. 1991. Examination of surface exposure ages of Antarctic moraines using in situ produced [10]Be and [26]Al. *Geochimica et Cosmochimica Acta* **55**(8): 2269–2283.

Brown ET, Stallard RF, Larsen MC, Raisbeck GM, Yiou F. 1995. Denudation rates determined from the accumulation of in situ-produced [10]Be in the Luquillo experimental forest, Puerto Rico. *Earth and Planetary Science Letters* **129**(1–4): 193–202.

Bussy F, Schaltegger U, Marro C. 1989. The age of the Mont Blanc granite (Western Alps): a heterogeneous isotopic system dated by Rb-Sr whole rock determinations on its microgranular enclaves. *Schweizerische Mineralogische und Petrographische Mitteilungen* **69**: 3–13.

Bussy F, Hernandez J, von Raumer JF. 2000. Bimodal magmatism as a consequence of the post-collisional readjustment of the thickened Variscan continental lithosphere (Aiguilles Rouges–Mont Blanc Massifs, Western Alps). *Geological Society of America Special Papers* **350**: 221–233.

Carretier S, Regard V, Vassalo R, Aguilar G, Martinod J, Riquelme R, Pepin E, Charrier R, Herail G, Farias M, Guyot JL, Vargas G, Lagane C. 2013. Slope and climate variability control of erosion in the Andes of central Chile. *Geology* **41**(2): 195–198.

Champagnac JD, Molnar P, Sue C, Herman F. 2012. Tectonics, climate, and mountain topography. *Journal of Geophysical Research* **117**: B02403.

Chmeleff J, von Blanckenburg F, Kossert K, Jakob D. 2010. Determination of the [10]Be half-life by multicollector ICP-MS and liquid scintillation counting. *Nuclear Instruments and Methods in Physics Research Section B* **268**(2): 192–199.

Church M, Ryder JM. 1972. Paraglacial sedimentation: a consideration of fluvial processes conditioned by glaciation. *Geological Society of America Bulletin* **83**: 3059–3072.

Codilean AT, Fenton CR, Fabel D, Bishop P, Xu S. 2014. Discordance between cosmogenic nuclide concentrations in amalgamated sands and individual fluvial pebbles in an arid zone catchment. *Quaternary Geochronology* **19**: 173–180.

Delmas M, Calvet M, Gunnell Y. 2009. Variability of Quaternary glacial erosion rates: a global perspective with special reference to the Eastern Pyrenees. *Quaternary Science Reviews* **28**: 484–498.

Delunel R, van der Beek PA, Carcaillet J, Bourlès DL, Valla PG. 2010. Frost-cracking control on catchment denudation rates: insights from in situ produced [10]Be concentrations in stream sediments (Ecrins–Pelvoux massif, French Western Alps). *Earth and Planetary Science Letters* **293**(1–2): 72–83.

Delunel R, van der Beek PA, Bourlès DL, Carcaillet J, Schlunegger F. 2014. Transient sediment supply in a high-altitude alpine environment evidenced through a [10]Be budget of the etages catchment (French Western Alps). *Earth Surface Processes and Landforms* **39**(7): 890–899.

Derrieux F, Siame LL, Bourlès DL, Chen RF, Braucher R, Léanni L, Lee JC, Chu HT, Byrne TB. 2014. How fast is the denudation of the Taiwan mountain belt? Perspectives from in situ cosmogenic [10]Be. *Journal of Asian Earth Sciences* **88**: 230–245.

Dielforder A, Hetzel R. 2014. The deglaciation history of the Simplon region (southern Swiss Alps) constrained by [10]Be exposure dating of ice-molded bedrock surfaces. *Quaternary Science Reviews* **84**: 26–38.

Dunai TJ. 2010. *Cosmogenic Nuclides: Principles, Concepts and Applications in the Earth Surface Sciences*. Cambridge University Press: Cambridge, UK.

Dunai TJ, Stuart FM. 2009. Reporting of cosmogenic nuclide data for exposure age and erosion rate determinations. *Quaternary Geochronology* **4**(6): 437–440.

Fallourd R, Harant O, Trouve E, Nicolas J-M, Gay M, Walpersdorf A, Mugnier J-L, Serafini J, Rosu D, Bombrun L, Vasile G, Vernier F, Tupin F, Moreau L, Bolon P. 2011. Monitoring temperate glacier displacement by multi-temporal TerraSAR-X images and continuous GPS measurements. *IEEE Journal of Selected Topics in Applied Earth Observations and Remote Sensing* **4**(2): 372–386.

Godon C. 2013. *L'érosion dans les environnements glaciaires: exemple du glacier des Bossons (Massif du Mont-Blanc, Haute-Savoie, France)*. PhD thesis, Université de Grenoble.

Godon C, Mugnier J, Fallourd R, Paquette J, Pohl A, Buoncristiani J. 2013. The Bossons glacier protects Europe's summit from erosion. *Earth and Planetary Science Letters* **375**: 135–147.

Goehring BM, Schaefer JM, Schluechter C, Lifton NA, Finkel RC, Jull AT, Akcar N, Alley RB. 2011. The Rhone Glacier was smaller than today for most of the Holocene. *Geology* **39**(7): 679–682.

Goehring BM, Vacco DA, Alley RB, Schaefer JM. 2012. Holocene dynamics of the Rhone Glacier, Switzerland, deduced from ice flow models and cosmogenic nuclides. *Earth and Planetary Science Letters* **351–352**: 27–35.

Guillon H, Godon C, Goupy B, Pohl A, Buoncristiani JF, Mugnier JL. 2013. Glacial and periglacial erosion rate inferred from five years of detrital flux monitoring (Bossons stream, Mont-Blanc massif, France). In *8th International conference (AIG) on Geomorphology*, International Association of Geomorphologists: Paris.

Haeberli W. 1976. Eistemperaturen in den Alpen. *Zeitschrift für Gletscherkunde und Glazial-geologie* **11**(2): 203–220.

Hallet B, Hunter L, Bogen J. 1996. Rates of erosion and sediment evacuation by glaciers: a review of field data and their implications. *Global and Planetary Change* **12**: 213–235.

Heimsath AM, McGlynn R. 2008. Quantifying periglacial erosion in the Nepal high Himalaya. *Geomorphology* **97**: 5–23.

Heisinger B, Niedermayer M, Hartmann FJ, Korschinek G, Nolte E, Morteani G, Neumaier S, Petitjean C, Kubik P, Synal A, Ivy-Ochs S. 1997. In-situ production of radionuclides at great depths. *Nuclear Instruments and Methods in Physics Research Section B* **123**(1–4): 341–346.

Heisinger B, Lal D, Jull A, Kubik P, Ivy-Ochs S, Knie K, Nolte E. 2002a. Production of selected cosmogenic radionuclides by muons. 2. Capture of negative muons. *Earth and Planetary Science Letters* **200**(3–4): 357–369.

Heisinger B, Lal D, Jull A, Kubik P, Ivy-Ochs S, Neumaier S, Knie K, Lazarev V, Nolte E. 2002b. Production of selected cosmogenic radionuclides by muons. 1. Fast muons. *Earth and Planetary Science Letters* **200**(3–4): 345–355.

Hinderer M, Kastowski M, Kamelger A, Bartolini C, Schlunegger F. 2013. River loads and modern denudation of the alps: a review. *Earth-Science Reviews* **118**: 11–44.

Huss M, Farinotti D. 2012. Distributed ice thickness and volume of all glaciers around the globe. *Journal of Geophysical Research* **117**(4): F04010.

Koppes MN, Montgomery DR. 2009. The relative efficacy of fluvial and glacial erosion over modern to orogenic timescales. *Nature Geoscience* **2**(9): 644–647.

Korschinek G, Bergmaier A, Faestermann T, Gerstmann U, Knie K, Rugel G, Wallner A, Dillmann I, Döllinger G, Gostomski LV, Kossert K, Maiti Moumita, Poutivtsev M, Remmert A. 2010. A new value for the half-life of ^{10}Be by heavy-ion elastic recoil detection and liquid scintillation counting. *Nuclear Instruments and Methods in Physics Research Section B* **268**(2): 187–191.

Lal D. 1991. Cosmic ray labeling of erosion surfaces: in situ nuclide production rates and erosion models. *Earth and Planetary Science Letters* **104**(2–4): 424–439.

Le Meur E, Vincent C. 2006. Monitoring of the Taconnaz ice fall (French Alps) using measurements of mass balance, surface velocities and ice cliff position. *Cold Regions Science and Technology* **46**(1): 1–11.

Lüthi MP, Bauder A. 2010. Analysis of Alpine glacier length change records with a macroscopic glacier model. *Geographica Helvetica* **65**: 92–102.

Merchel S, Herpers U. 1999. An update on radiochemical separation techniques for the determination of long-lived radionuclides via accelerator mass spectrometry. *Radiochimica Acta* **84**: 215–219.

Molnar P, England P. 1990. Late Cenozoic uplift of mountain ranges and global climate change: chicken or egg? *Nature* **346**: 29–34.

Montgomery DR. 2002. Valley formation by fluvial and glacial erosion. *Geology* **30**(11): 1047–1050.

Nussbaumer SU, Zumbühl HJ. 2012. The Little Ice Age history of the glacier des Bossons (Mont Blanc massif, France): a new high-resolution glacier length curve based on historical documents. *Climatic Change* **111**: 301–334.

Paquette JL, Menot RP, Peucat JJ. 1989. Sm-Nd and U-Pb zircon study of eclogites from the Alpine External Massifs (Western Alps): evidence for crustal contamination. *Earth and Planetary Science Letters* **96**: 181–198.

Parker G, Perg LA. 2005. Probabilistic formulation of conservation of cosmogenic nuclides: effect of surface elevation fluctuations on approach to steady state. *Earth Surface Processes and Landforms* **30**(9): 1127–1144.

Pedersen VK, Egholm DL. 2013. Glaciations in response to climate variations preconditioned by evolving topography. *Nature* **493**(7431): 206–210.

Prud'homme C. 2013. *Géomorphologie glaciaire et nucléides cosmogéniques. Qu'est-ce que l'on date?* Master's thesis, Université Joseph Fourrier, Grenoble.

Rey F. 2004. *Crash au Mont-Blanc*. Glénat: Grenoble.

Roe GH, O'Neal MA. 2005. The response of glaciers to intrinsic climate variability: observations and models of late-Holocene variations in the Pacific Northwest. *Journal of Glaciology* **55**: 839–854.

Savi S, Norton K, Picotti V, Brardinoni F, Akçar N, Kubik P, Delunel R, Schlunegger F. 2014. Effects of sediment mixing on ^{10}Be concentrations in the Zielbach catchment, central-eastern Italian Alps. *Quaternary Geochronology* **19**: 148–162.

Schaefli B, Hingray B, Niggli M, Musy A. 2005. A conceptual glacio-hydrological model for high mountainous catchments. *Hydrology and Earth System Sciences Discussions* **2**: 73–117.

Scherler D, Bookhagen B, Strecker MR. 2014. Tectonic control on ^{10}Be-derived erosion rates in the Garhwal Himalaya, India. *Journal of Geophysical Research: Earth Surface* **119**(2): 83–105.

Seong YB, Owen LA, Caffee MW, Kamp U, Bishop MP, Bush A, Copland L, Shroder JF. 2009. Rates of basin-wide rockwall retreat in the K2 region of the Central Karakoram defined by terrestrial cosmogenic nuclide ^{10}Be. *Geomorphology* **107**(3–4): 254–262.

Slaymaker O. 2011. Criteria to distinguish between periglacial, proglacial and paraglacial environments. *Quaestiones Geographicae* **30**(1): 85–94.

Sternai P, Herman F, Valla PG, Champagnac JD. 2013. Spatial and temporal variations of glacial erosion in the Rhône valley (Swiss Alps): insights from numerical modeling. *Earth and Planetary Science Letters* **368**: 119–131.

Stone JO. 2000. Air pressure and cosmogenic isotope production. *Journal of Geophysical Research* **105**(B10): 23753.

Suter S. 2001. *Cold firn and ice in the Monte Rosa and Mont Blanc areas: spatial occurrence, surface energy balance and climatic evidence*. PhD thesis, Swiss Federal Institute of Technology, Zürich.

Suter S, Hoelzle M. 2002. Cold firn in the Mont Blanc and Monte Rosa areas, European Alps: spatial distribution and statistical models. *Annals of Glaciology* **35**(1): 9–18.

van der Veen CJ. 2007. Fracture propagation as means of rapidly transferring surface meltwater to the base of glaciers. *Geophysical Research Letters* **34**(1): L01501.

Vincent C, Le Meur E, Six D, Possenti P, Lefebvre E, Funk M. 2007. Climate warming revealed by englacial temperatures at Col du Dôme (4250 m, Mont Blanc area). *Geophysical Research Letters* **34**(16): L16502.

Vivian R. 1969. Les glaciers des Bossons et de Taconna. *Revue de Géographie Alpine* **57**: 871–874.

von Blanckenburg F. 2005. The control mechanisms of erosion and weathering at basin scale from cosmogenic nuclides in river sediment. *Earth and Planetary Science Letters* **237**(3–4): 462–479.

Ward DJ, Anderson RS. 2011. The use of ablation-dominated medial moraines as samplers for ^{10}Be-derived erosion rates of glacier valley walls, Kichatna Mountains, AK. *Earth Surface Processes and Landforms* **36**(4): 495–512.

Appendix A ^{10}Be Production under Bossons Glacier

Terrestrial cosmogenic nuclides (TCNs) are produced by reactions between cosmic ray particles and element targets at the surface of the Earth. Three mechanisms produce cosmogenic ^{10}Be: spallation due to interaction with primary neutrons; negative and slow muon capture; fast muon interaction (i.e. Bremsstrahlung), giving rise to secondary neutrons (i.e. photoneutrons) (Dunai, 2010). TCN concentrations are impacted by altitude and latitude of the sampling location. Altitude scaling is performed by using the following relation to calculate pressure at the sampling site:

$$P(z) = P_s \exp\left(-\frac{gM}{R\xi}\left[\ln T_s - \ln(T_s - \xi z)\right]\right) \quad \text{(A1)}$$

with P_s the sea-level standard pressure (P_s = 1013.25 hPa), g the gravitational acceleration (g = 9.80665 m s^{-2}), M the molar mass of air (M = 28.97×10^{-3} kg mol^{-1}), R the ideal gas constant (R = 8.3144621 J mol^{-1} K^{-1}), T_s the sea-level standard temperature (T_s = 288.15 K) and ξ the adiabatic gradient (ξ = 0.0065 K m^{-1}).

Production scaling with latitude is then performed through the well-known Lal (1991) polynomial relations:

Table A1.   TCN production parameters

Parameter	Value	Reference
Latitude	45.88°	This study
Ice density	865.85 kg m^3	This study
$\Pi_{n,HLSL}$	4.33 ± 0.21 atom g^{-1}	Balco *et al.* (2008)
Λ_n	150 g cm^{-2}	Braucher *et al.* (2003)
$\Lambda_{\mu,slow}$	1500 g.cm^{-2}	Braucher *et al.* (2003)
$\Lambda_{\mu,fast}$	5300 g.cm^{-2}	Braucher *et al.* (2003)
f_n	97.85%	Braucher *et al.* (2003)
$f_{\mu,fast}$	0.65%	Braucher *et al.* (2003)
$f_{\mu,slow}$	1.5%	Braucher *et al.* (2003)
$f_C(SiO_{2O})$	0.704	Heisinger *et al.* (2002a)
$f_D(SiO_{2O})$	0.1828	Heisinger *et al.* (2002a)
$f^*(^{10}Be)$	0.43 ± 0.03%	Heisinger *et al.* (2002a)

$$\alpha_{tot} = f_n \alpha_n + (1 - f_n)\alpha_\mu \quad \text{(A2)}$$

$$\alpha_n(P) = a + b \exp-\frac{P}{150} + cP + dP^2 + eP^3 \quad \text{(A3)}$$

$$\alpha_\mu(P) = M_{\lambda,1013.25} \exp\frac{1013.25 - P}{242} \quad \text{(A4)}$$

where α_{tot}, α_n and α_μ are the scaling factors for all particles, neutrons and muons (slow and fast together), respectively, f_n is the proportion of neutrons in the incoming particle flux, P the pressure at the sampling location given by relation (A1) and a, b, c, d, e and $M_{\lambda,1013.25}$ are scaling coefficients depending on latitude and given by Stone (2000) from Lal (1991). Production for each mechanism can then be inferred using following relations:

$$\Pi_s = \frac{\Pi_{n,HLSL}}{f_n} \quad \text{(A5)}$$

$$\Pi_{tot} = \alpha_{tot} \quad \text{(A6)}$$

$$\Pi_n = f_n \Pi_{tot} \quad \text{(A7)}$$

$$\Pi_{\mu,fast} = f_{\mu,fast} \Pi_{tot} \quad \text{(A8)}$$

$$R_{\mu,slow} = f_{\mu,slow} \Pi_{tot} \quad \text{(A9)}$$

with $\Pi_{n,HLSL}$ neutronic production at high latitude and sea level, Π_s total standard production at high latitude and sea level, Π_{tot} total scaled production at sampling location, $\Pi_n, \Pi_{\mu,fast}$ neutron and fast muon scaled production, respectively, $R_{\mu,slow}$ slow muon stopping rate, $f_n, f_{\mu,slow}$ and $f_{\mu,fast}$ proportion of neutrons, slow muons and fast muons in the incoming particle flux, respectively.

The following relations (Heisinger *et al.*, 2002a, 2002b) yield production scaled with penetration depth and density of the material:
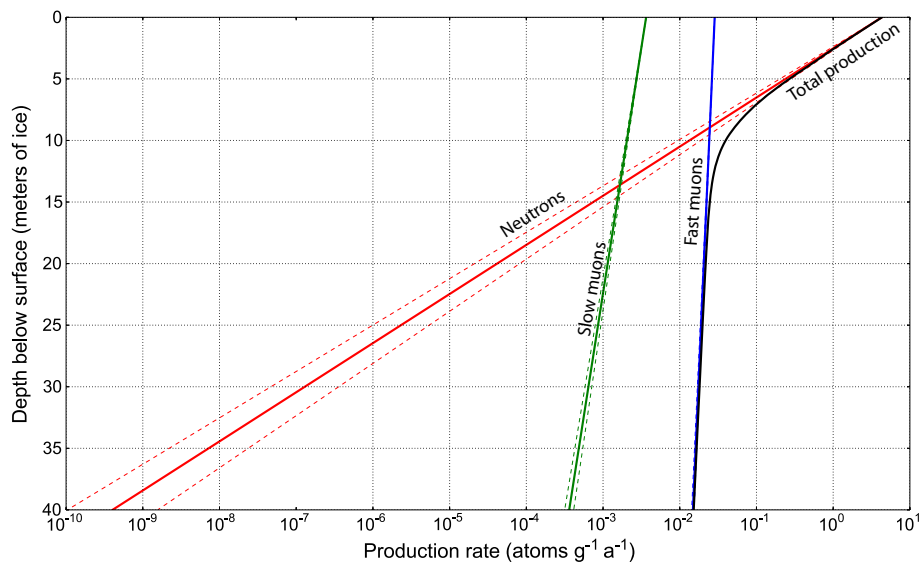
$$\Pi_n(\delta) = \Pi_n(0) \exp-\frac{\rho\delta}{\Lambda_n} \quad \text{(A10)}$$

$$\Pi_{\mu,fast}(\delta) = \Pi_{\mu,fast}(0) \exp-\frac{\rho\delta}{\Lambda_{\mu,fast}} \quad \text{(A11)}$$

$$R_{\mu,slow}(\delta) = R_{\mu,slow}(0) \exp-\frac{\rho\delta}{\Lambda_{\mu,slow}} \quad \text{(A12)}$$

Figure A1. ^{10}Be production rate under ice at sea level and 45° latitude for loosely compacted ice (ρ = 815 kg m^{-3}, upper dashed line), well-compacted ice (ρ = 916.7 kg m^{-3}, lower dashed line) and a mean value (ρ = 865.85 kg m^{-3}, solid line). This figure is available in colour online at wileyonlinelibrary.com/journal/espl

$$\Pi_{\mu,\text{slow}}(\delta) = R_{\mu,\text{slow}}(\delta)f_C(Z_t)f_D(Z_t)f^*(^AZ) \qquad (A13)$$

where Λ_n, $\Lambda_{\mu,\text{fast}}$ and $\Lambda_{\mu,\text{slow}}$ are the attenuation lengths for neutrons, fast muons and slow muons, respectively, $f_C(Z_t)$ the chemical compound factor, $f_D(Z_t)$ is the probability that the negative muon does not decay in the K-shell before nuclear capture, $f^*(^AZ)$ is the effective probability for production of nuclide ^AZ after capture, ρ is material density and δ is penetration depth (ρ and δ are often assembled as one term $h = \rho\delta$). Relations (A1)–(A13) allow calculation of TCN production attenuation through ice. Figure A1 presents such results at sea level and high latitude for loosely compacted ice ($\rho = 815$ kg m^{-3}), well-compacted ice ($\rho = 916.7$ kg m^{-3}) and a mean value ($\rho = 865.85$ kg m^{-3}). Production is almost non-existent under ~15 m of ice. Parameter values used in our calculation are given in Table A1.

Huss and Farinotti (2012) estimated ice thickness with a 25 m horizontal resolution for almost 200 000 glaciers worldwide. Their computation for the Bossons glacier provided insights into its ice thickness, which varies from 30 m near the front, sides and rock outcrops to almost 180 m at Grand Plateau and east to Pic Wilson (Figures 1 and A2). The ice thickness distribution of Bossons glacier (Figure A3) shows that the majority of the glacier is over 30 m thick. Production rates should therefore be very low under the Bossons glacier.

Relatively high production rates (~1 atom g^{-1} a^{-1}) near glacial termini or rock outcrops may significantly impact TCN concentrations measured from subglacial stream sediments. Using the ice thickness inferred by Huss and Farinotti (2012) and relations (A1)–(A13) allows calculation of present-day production rates under the Bossons glacier (Figure A4). If erosion rate was constant and if a single subglacial stream were
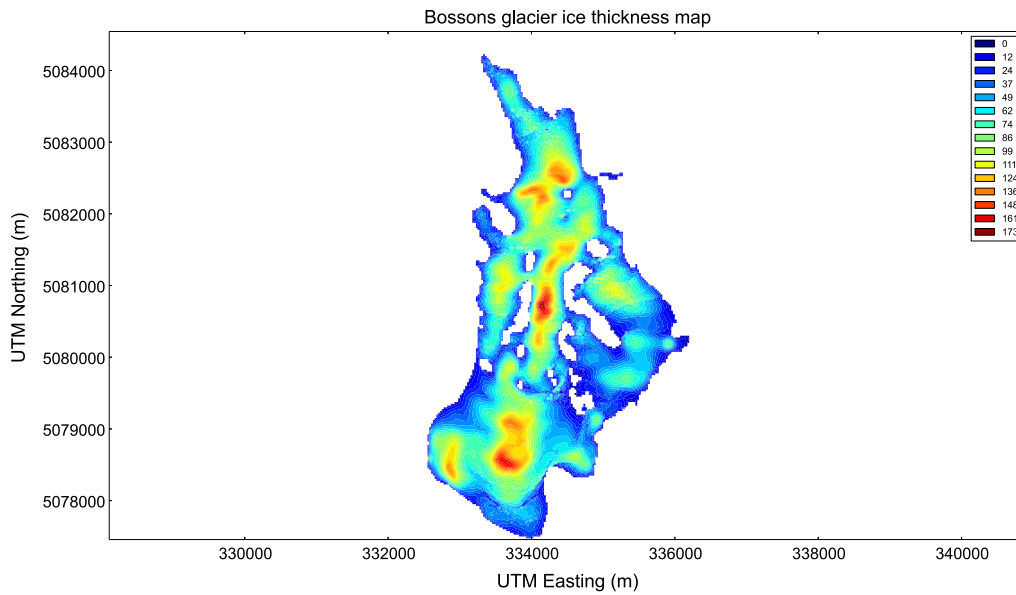

Figure A2. Bossons glacier ice thickness calculated using output of Huss and Farinotti (2012) model. Ice thickness in meters. This figure is available in colour online at wileyonlinelibrary.com/journal/espl
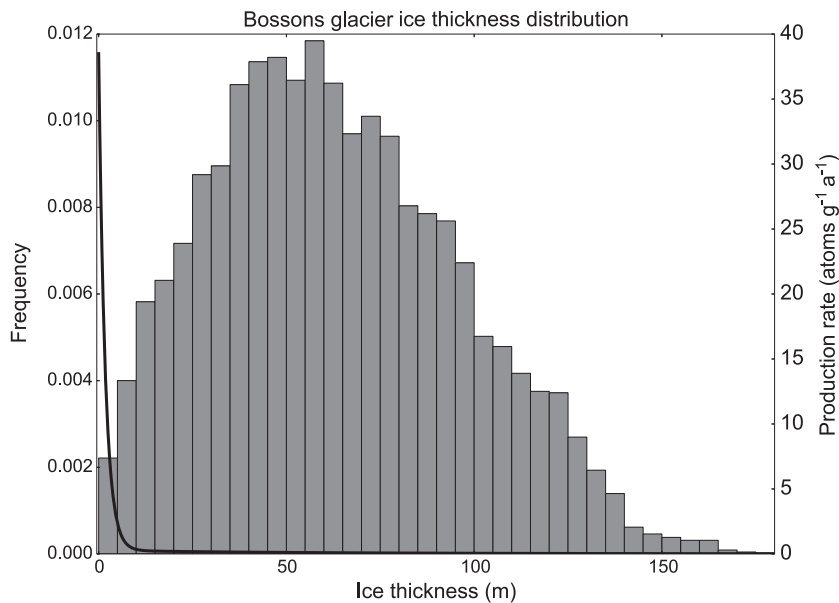
Figure A3. Bossons glacier ice thickness distribution in 5 m bins. Solid line corresponds to total ^{10}Be production rate under ice at 2800 m asl and a latitude of 45.88°.
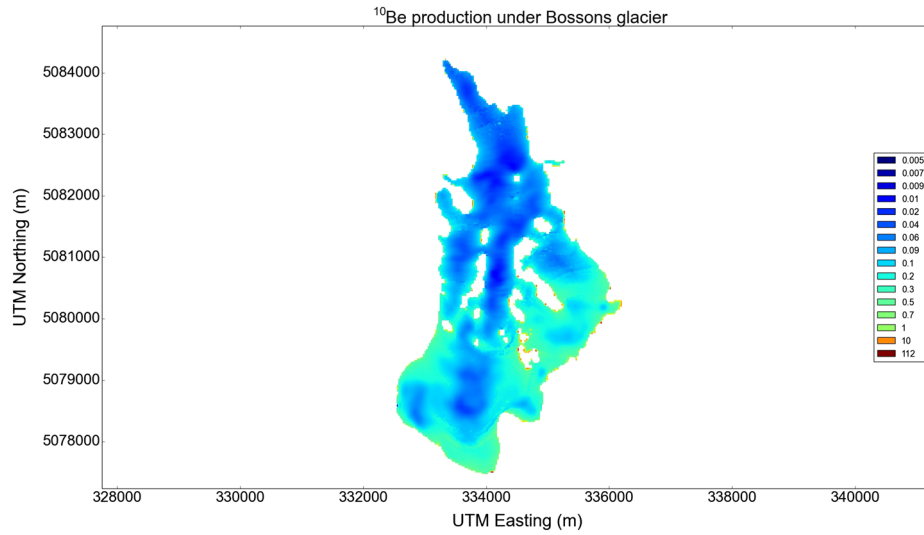
Figure A4. ^{10}Be production under Bossons glacier calculated using thickness from the Huss and Farinotti (2012) model and relations (A1–A13). Production rates are given in atoms g^{-1} a^{-1}. This figure is available in colour online at wileyonlinelibrary.com/journal/espl
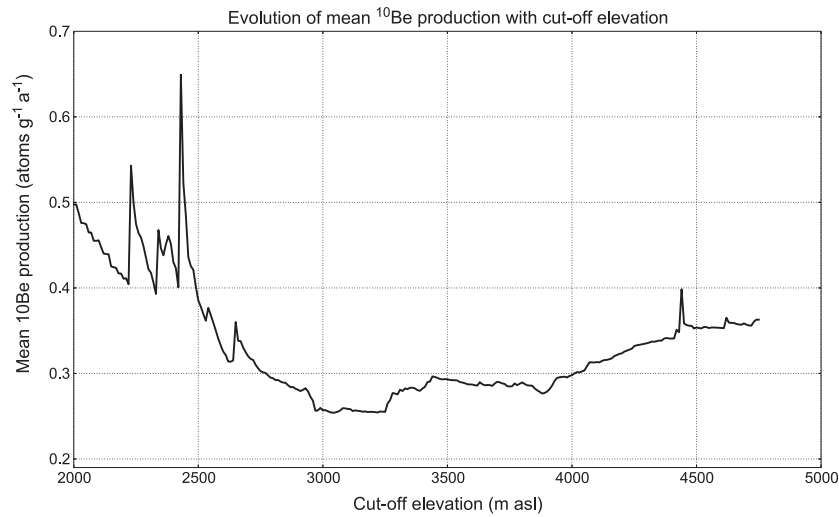
Figure A5. Evolution of mean production in subglacial stream with cut-off elevation.

to drain the entire subglacial catchment up to an elevation z_c, the measured concentration would be a mean production rate times exposure duration. Production rates from Figure A4 allow calculation of a mean ^{10}Be production rate $\bar{\Pi}$, with cut-off elevation z_c:

$$\bar{\Pi}(z_c) = \sum_{i=1}^{n(z_c)} \frac{\Pi_i}{n(z_c)} \qquad (A14)$$

with $n(z_c)$ the number of cells in the Huss and Farinotti (2012) model for a given cut-off elevation z_c and Π_i the production of the ith cell.

Results of such calculations are shown in Figure A5. $\bar{\Pi}(z_c)$ peaks are related to glacier thinning near its sides and rock outcrops. Mean production over the whole glacier is $\sim$0.33 atom g^{-1} a^{-1}. Integrating this value over the Holocene ($\sim$12 ka) yields a concentration of 3.96×10^3 atoms g^{-1}.